Journal of Inorganic and Organometallic Polymers and Materials (2022) 32:2455–2472
https://doi.org/10.1007/s10904-022-02365-2

# Sorption of Palladium(II) from Aqueous Solution Using Diphenylthiocarbazone Immobilized onto Kieselguhr

**R. Gamal[1] · S. E. Rizk[1] · N. E. El-Hefny[1]**

Received: 30 November 2021 / Accepted: 3 May 2022 / Published online: 26 May 2022


**Abstract**
Kieselguhr was immobilized with diphenylthiocarbazone (dithizone) and utilized as a new sorbent to extract palladium ions from an aqueous solution. The physicochemical features of the immobilized kieselguhr (K–Dz) were specified by Fourier transform infrared spectroscopy, scanning electron microscopy, energy dispersive X-ray spectroscopy and thermogravimetric analysis–differential thermal analysis. The average crystal size of the prepared material was found to be 24.41 nm. The sorption potential of the immobilized kieselguhr for the extraction of Pd(II) and La(III) in a batch mode was studied. The effects of pH, shaking time as well as the initial concentration of metals have been examined. The results demonstrate that the optimum pH was found to be 4.5 and the equilibrium was attained within 15.0 min. The adsorption kinetics and equilibrium data were well described by the pseudo-second-order kinetic model and Sips isothermal model with a maximum sorption capacity of 20.3 (mg/g). Thermodynamic parameters of the studied metal ions show that the process is spontaneous and endothermic in nature. The desorption process of Pd(II) was highly managed using acidified thiourea giving a desorption percent of approximately 80.0%. The separation possibility of Pd(II) from some metal ions such as La(III) was achieved successfully. The developed (K–Dz) composite method was applied for the recovery and separation of Pd(II) and other metal ions from a simulated automotive catalyst leachate solution. The results indicated that the (K–Dz) composite has a good reusability potential.

**Keywords** Sorption · Palladium(II) · Lanthanum(III) · Kieselguhr · Dithizone · Automotive catalyst

## 1 Introduction

Palladium (Pd) plays a key role in many applications owing to its outstanding physicochemical properties such as thermal stability, high conductivity and catalytic properties [1]. It is used extensively with rare earth elements in electronic and medical devices as well as in automotive catalytic converters [2]. However, the production of palladium from ore mining is quite low while it is considered one of the most important fission products which are produced with high yields together with rare earth elements in radioactive effluents [3]. In this context, recovering and separating of palladium from fission products and industrial waste are critical to meet the growing demand for this valuable metal. Various methods have been employed to recover the palladium including solvent extraction [4], chemical precipitation [5] and ion exchange/sorption [6, 7]. Compared to other methods; the sorption technique provides several advantages, especially for metal recovery in dilute aqueous solutions. Diatomaceous silica or kieselguhr ($SiO_2$) has attracted attention as a contaminant scavenger due to its high specific surface area, low bulk density, high permeability and porosity with excellent mechanical and thermal stability [8]. Emam et al. [9] reported that the adsorptive removal of the rare earth elements from sulfate medium by kieselguhr was successfully improved by impregnating its surface with Cyanex 572. Although the selective separation of palladium is still challenging, adsorbents functionalized with sulfur and nitrogen donor atoms are widely studied for the effective separation of Pd(II) from other co-existing metal ions. Yamada et al. [10] studied the separation of Pd(II) from spent automotive catalysts containing different metal ions at pH 0.5 using 1,3-bis(2-(octylthio)propan-2-yl) benzene impregnated Amberlite XAD-7 resin. They found that the impregnated resin bonded specifically to Pd(II)

✉ R. Gamal
chemist_rgn@yahoo.com

[1] Hot Laboratories Center, Egyptian Atomic Energy Authority, Cairo 13759, Egypt

through sulfur–carbon–sulfur (SCS) coordination achieving high selectivity > 90% over the leachate of the spent automotive catalyst. Ruhela et al. [11] synthesized Acetyl amide grafted XAD-16 for the removal of palladium and other metal ions from high-level waste (HLW). They found that the sorption kinetics of Pd onto the resin was fast and the resin has shown higher sorption of Pd(II) with small extraction of rare earth elements (REEs) relative to other elements. Spies and Wewers [12] reported the efficiency of the Cd(II) sorbed onto a modified dithizone-impregnated Amberchrom CG-300m polymer resin. They showed that the modified Amberchrom CG-300m is effective for the removal of Cd(II) ions from dilute aqueous solutions. Successful synthesis of nano-composites was performed and analyzed using different techniques by several researchers [13–16]. Surface modification of the porous silica with organic substances arises in the formation of a hybrid with desirable physicochemical properties of both organic and inorganic materials required in advanced applications [17–19]. The objective of this current work was to study the synthesis of dithizone immobilized onto kieselguhr (K–Dz) as a new sorbent and its extraction and separation behavior for Pd(II) and La(III) ions from aqueous chloride media. Kieselguhr was fully characterized before and after the immobilizing by dithizone using different techniques. Furthermore, kinetics, adsorption isotherms as well as thermodynamic studies were performed for elucidating the nature and mechanism of Pd(II) and La(III) sorbed by (K–Dz) composite. Finally, the immobilized kieselguhr was usefully applied for a selective recovery towards Pd(II) and La(III) from synthetic leach liquors of automotive catalysts.

## 2 Experimental

### 2.1 Materials and Reagents

Unless otherwise stated, all reagents were of high purity and were used as supplied without any further purification. White kieselguhr was purchased from the British Drug House Limited (BDH, England). Dithizone was supplied from Winlab, China. Lanthanum chloride heptahydrate, ammonium ceric nitrate, toluene and ethanol were obtained from Merck, Germany. Palladium chloride ($PdCl_2$) was a Fluka product, Germany. HCl and NaOH were supplied from BDH, England. Potassium iodide, ascorbic acid and aluminum nitrate nonahydrate were supplied from Sigma-Aldrich, Germany. Bidistilled water was used for all experiments.

### 2.2 Instrumentation

The measurements of hydrogen ion concentration were conducted using a Hanna pH-meter with a resolution of 0.01 and accuracy of ± 0.01. A Shimadzu UV/visible double beam spectrophotometer of model UV-160A, (Japan) was utilized to quantify the concentration of Pd(II) solution using the iodide method at λ = 407 ± 3 nm [20]. The structure of the kieselguhr before and after dithizone immobilization was characterized by X-ray diffraction (XRD) spectroscopy and the patterns were recorded by a diffractometer Shimadzu XD-Dl, Japan with a Cu Kα-X-radiation source (λ = 1.5418 Å) in a diffraction angle (2θ) range between 4.0° and 90°. The Fourier transform infrared (FTIR) spectra for the kieselguhr, (K–Dz) composite before and after loading with the palladium ions were gained by using a 2000 FT-IR, Perkin Elmer Co., USA spectrometer spectral range of 400–4000 $cm^{-1}$. The surface morphology of the composite and its origin as well after its binding with Pd(II) were visualized by scanning electron microscopy (SEM) by a JOEL-JSM-6510 LA electronic microscope. The elemental composition of the composite was identified by an energy dispersive X-ray spectroscopy (EDX) equipped on SEM, JSM-5600LV Oxford, JEOL (Japan). Thermogravmetric analysis (TGA) and differential thermal analysis (DTA) of the composite were carried out at a heating rate of 10 °C/min using a DTG-60/60H thermal analyzer (Shimadzu, Kyoto, Japan).

### 2.3 Preparation of Kieselguhr–Dithizone Composite

The immobilization of dithizone onto kieselguhr was carried out by a physical impregnation method at 50 °C to avoid dithizone oxidation [21]. Firstly, as referred by Marzenko [20] dithizone was purified before use to eliminate the oxidation products. The pure stabilized dithizone was obtained by shaking in chloroform solution with a diluted ammonia solution (1.0%). The ammoniacal extract was separated from the chloroform phase and acidified with dilute HCl to precipitate the dithizone. Finally, dithizone was washed with bidistilled water and the solvent was evaporated in a water bath at 50 ± 1 °C. Kieselguhr–dithizone (K–Dz) composite was prepared as the earlier reported procedure [21]. Briefly, 5.0 g of kieselguhr was added to 1.25 g dithizone in an 80 mL toluene solution. Then, the mixture was magnetically stirred for 24 h at 50 ± 1 °C. The obtained composite was filtered and washed successively with toluene, ethanol and water several times until the dark color of the dithizone was not observed in the filtrate. The synthesized (K–Dz) composite was dried at 60 °C for 8.0 h and the final weight of the dried (K–Dz) composite was 5.24 g. In addition, the visual examination shows a black color of the final product. A schematic illustration is represented in Fig. 1.

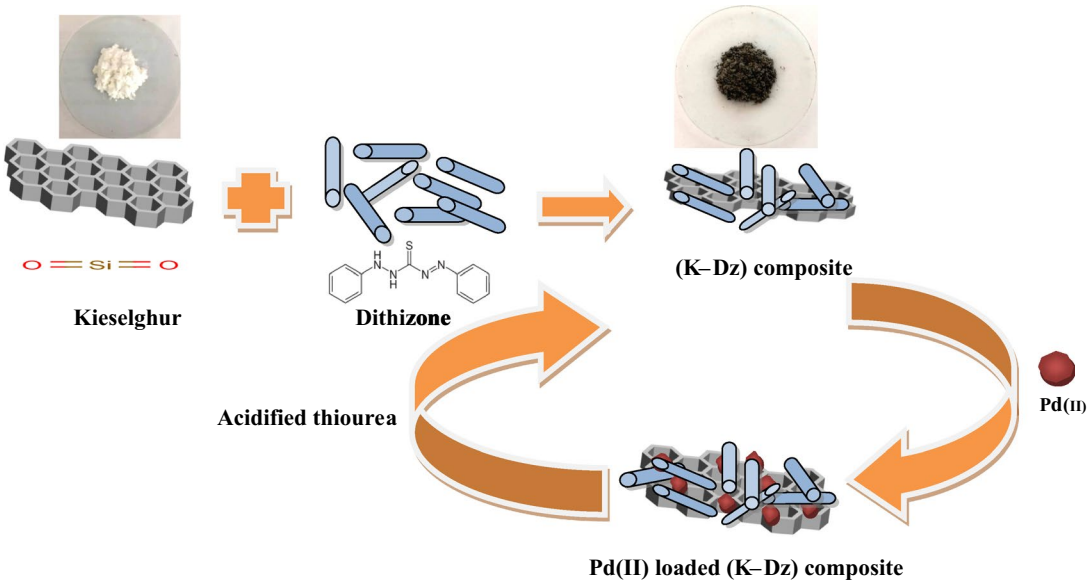


**Fig. 1** Schematic diagram of the prepared dithizone immobilized kieselguhr composite

## 2.4 Batch Sorption Tests

The stock Pd(II) and La(III) solutions (100 mg/L) were prepared by dissolving in 0.1 mol/L hydrochloric acid solution. Except if specified, sorption experiments were executed in batch systems by mixing 0.05 g of (K–Dz) with 5.0 mL of 100 mg/L Pd(II) and La(III) solutions using a thermostatically controlled water bath shaker where the temperature was set at 25 ± 1 °C. 0.01 mol/L NaOH and HCl solutions were used for the pH adjustment of the starting metal solutions. After a period of 15.0 min., which was a sufficient time for achieving the equilibrium, the samples were separated by filtration and the filtrate was analyzed for determination of the residual metals concentrations. The retention percent (R%) of metals and the sorption capacity of the (K–Dz) composite were estimated by the mass balance relationship:

$$R\ \% = \frac{(C_i - C_e)}{C_i} \times 100 \tag{1}$$

$$q_e = (C_i - C_e) \times \frac{V}{m} \tag{2}$$

where $C_i$ and $C_e$ (mg/L) are the initial and residual concentrations of Pd(II) or La(III), respectively; V is the solution volume expressed in (L) and m in (g) is the adsorbent weight.

For the desorption study, the sorbent was initially loaded with the palladium at the optimum condition. The amount of Pd(II) sorbed onto the sorbent was calculated. Then, the loaded sorbent was contacted with acidified thiourea, 1.0 mol/L of HCl as an eluent solution at a varied concentration from 0.1 to 2.0 mol/L thiourea, and the amount of Pd(II) eluted from the sorbent was computed. The desorption percentage (D%) was estimated from the ratio of the Pd(II) amounts in the eluted to that retained by the sorbent, as given by the following equation:

$$D\ (\%) = \frac{\text{Amount of Pd(II) desorbed}}{\text{Amount of Pd(II) sorbed}} \times 100 \tag{3}$$

## 2.5 Statistical Validation of the Kinetic and Isotherm Models Using Akaike Information Criterion (AIC)

A statistical comparison of the best representative fitting of the applied kinetic and isotherm models for the experimental data was evaluated by the Akaike information criterion (AIC) methodology [22]. According to the AIC approach, the model with the lowest value of AIC is selected as the best-suited model for the data among the specified models. The AIC value can be estimated from the following relationship:

$$AIC = 2P + Nln\left(\frac{SSE}{N}\right) \tag{4}$$

where P and N are the numbers of the model parameters and the observation points, respectively. SSE is the sum of square errors which was calculated as follows:

$$SSE = \sum_{i=1}^{N} \left(q_{e,exp} - q_{e,calc.}\right)^2 \tag{5}$$

### 2.6 Automotive Catalyst Analysis

The concentrations of the main chemical composition of the automotive catalyst in the aqueous phase have been taken regarding the work reported by Kimuro et al. [23]. It is composed of Al (312.92 mg/L), Ce (173.79 mg/L), La (17.13 mg/L), Pd (55.46 mg/L), Pt (2.65 mg/L) and Rh (3.73 mg/L). As reported by Li et al. [24], Ce(IV) exists as free ions in a highly acidic medium due to its high electric charge. Accordingly, at pH 4.5 Ce(IV) was easily hydrolyzed to form polynuclear hydroxo complex. The leaching process was performed by dissolving the aforementioned elements in an applicable amount of HCl and adjusting the pH value at 4.5. Then, filtrate the leach solution to get rid of Ce(IV) precipitate. Add 5.0 g of the (K–Dz) composite to the leach liquor solution with continuous shaking for 15.0 min. duration at 25 ± 1 °C. After leaching, the leach solution and the remaining insoluble residue were separated by filtration, and the residue was used for the sequential elution steps. The metal concentrations in the simulated leach solution were estimated after adequate dilution using ICPS-7500 Shimadzu Sequential Plasma Spectrometer, Kyoto, Japan.

## 3 Results and Discussion

Diphenylthiocarbazone or dithizone ($H_2Dz$) is a monobasic acid or a multidentate organic ligand containing one sulfur and four nitrogen donor atoms (soft bases) which makes it an efficient material for trace metals extraction. The immobilization of ($H_2Dz$) onto porous silica as sorbent material like kieselguhr well illustrates a useful adsorbent for the adsorption of trace amounts of different elements [25].

### 3.1 Physicochemical Characterization of Kieslguhr–Dithizone Composite

The immobilized ($H_2Dz$) was characterized by X-ray diffraction (XRD) analysis compared to the typical kieselguhr. Figure 2 shows the XRD patterns of kieselguhr and its composite with dithizone. Kieselguhr profile is very close to kieselguhr–dithizone composite as they had intense peaks at 2θ values of 21.9°, 28.5°, 31.4°, 36.4° which are associated with the crystalline phase of silica [8]. Besides the silica peaks, the composite pattern shows reflection peaks related to dithizone at 2θ values of 8.33° and 14.19° [26]. By examining the kieselguhr patterns before and after impregnation, it is possible to conclude that the immobilization of dithizone does not deform the kieselguhr structure. These results support that dithizone immobilized with kieselguhr was synthesized properly. Furthermore, the crystal size of (K–Dz) composite could be estimated by Scherrer's equation

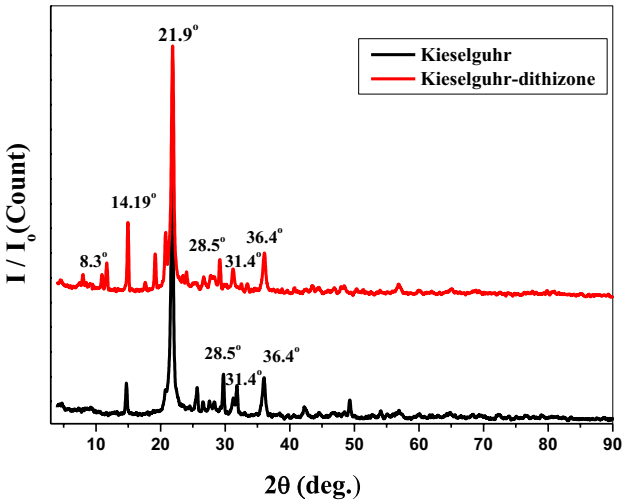


**Fig. 2** XRD patterns of kieselguhr and kieselguhr–dithizone composite

through the below relation between the crystal's size and the width of the line [27].

$$D = \frac{0.9\lambda}{\beta \cos\theta} \tag{6}$$

where D is the average crystal size in nm, λ is the specific wavelength of the incident X-ray (λ(Kα) = 1.540 Å), θ is the Bragg diffraction angle and β is the full width at half maxima of the diffraction peak. The average size of the (K–Dz) crystallite was calculated from the full width of half maxima of the diffraction peaks by fitting the reflected peaks with the Gaussian function and found to equal 24.41 nm.

Morphology and structure of the naked kieselguhr, (K–Dz) and (Pd–K–Dz) composite were examined by Scanning Electron Microscopy (SEM), Fig. 3. The micrographs of the blank kieselghur shows spherical particles arranged in a honeycomb porous structure along with rectangular-shaped fractions signifying the microporous silicate and the calcium sulphate existing in the kieselguhr, respectively Fig. 3a. After dithizone impregnation, the formation of a large quantity from straight long rods mixed with small amounts of shorter rods with a rough surface was observed in addition to the structure of the silicate, Fig. 3b. It was evident from this figure that there was no noticeable change in the surface morphology of the kieselguhr. This is related to the differences in the sorption behavior between the typical and immobilized kieselguhr depending on the functional groups of their surface, not on their morphologies. Fractal geometry was applied to the SEM images to characterize the surface structure and the irregularities of the pore distributions on the kieselguhr before and after dithizone impregnation. The pore distribution fractal dimension ($D_1$)

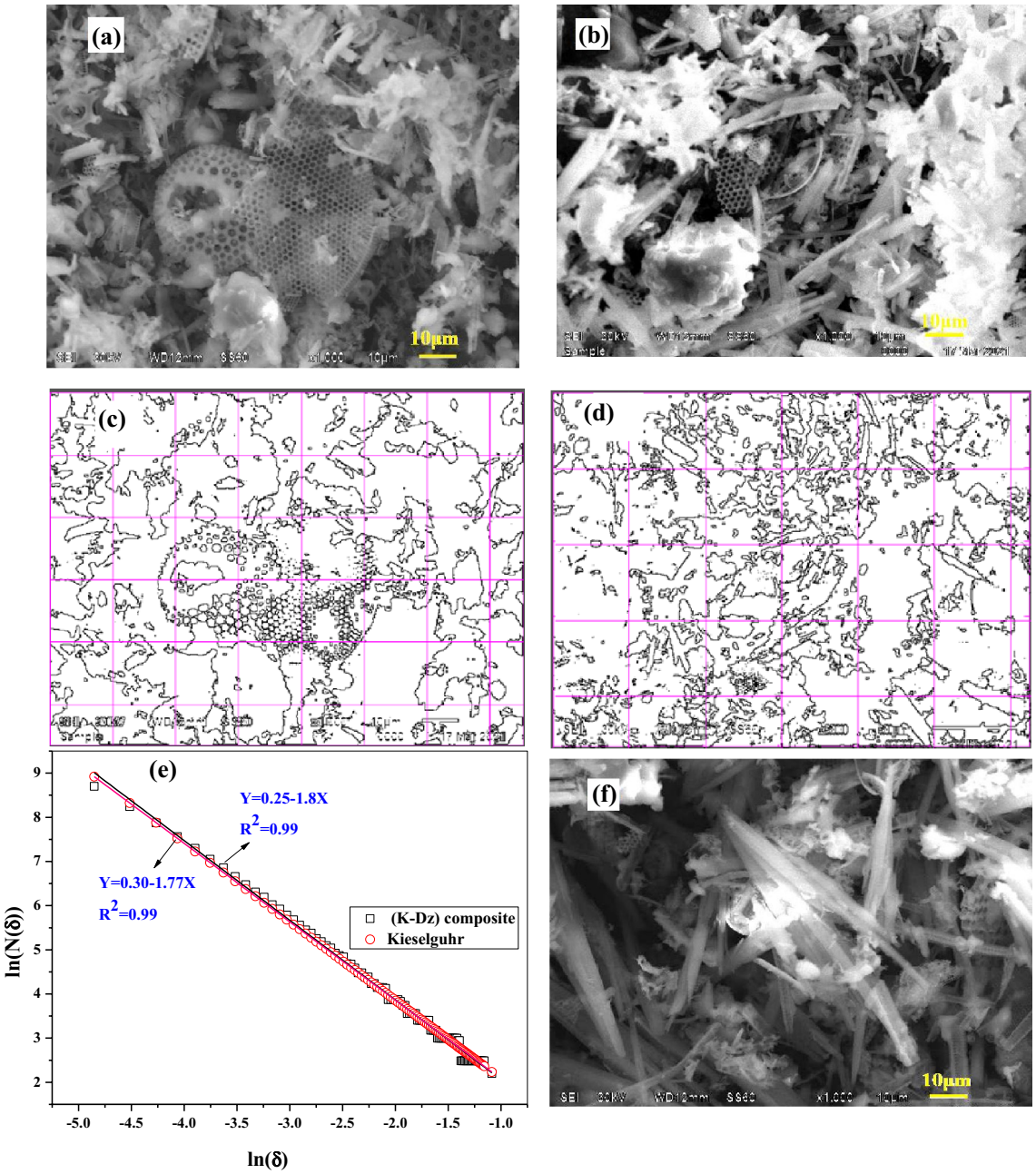


**Fig. 3** SEM image of: **a** Kieselguhr, **b** Kieselguhr–dithizone composite, surface coverage image using box counting method for fractal dimension of **c** Kieselguhr **d** Kieselguhr–dithizone composite **e** Fitting curve of surface fractal dimension of kieselguhr and (K–Dz) composite **f** SEM image of Pd(II) loaded kieselguhr–dithizone composite

was computed using box-counting method after the SEM photos were transformed into binary images with boxes of length, δ, $D_1$ can be calculated from the following linear relationship [28]:

$$\ln(N(\delta)) = -D_1 ln\delta + constant \quad (7)$$

where N (δ) is the number of boxes needed to cover the whole of the binary image.

Figure 3c and d depicts the binary SEM box coverage images of kieselguhr and (K–Dz) composite for the fractal dimension analysis and their regression analysis plot was shown in Fig. 3e. It was noticed that the plot displays good fitting with a high correlation coefficient > 0.99 indicating that the pore distribution of kieselghur and (K–Dz) composite are fractal. However, the value of $D_1$ of the composite is 1.8 which is higher than $D_1$ of kieselghur ($D_1 = 1.77$)

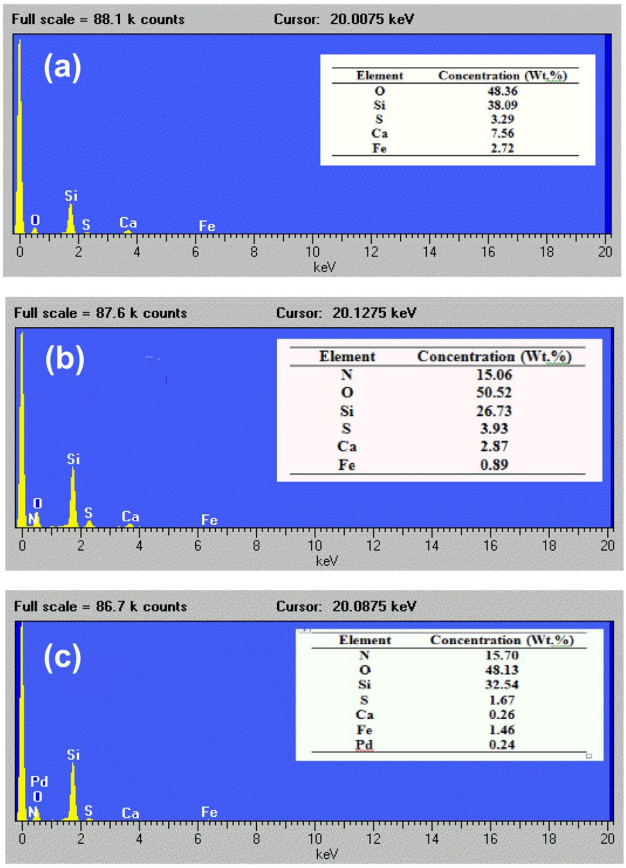


**Fig. 4** EDX spectra of: **a** Kieselguhr, **b** Dithizone immobilized kieselguhr, **c** Pd(II) loaded immobilized kieselguhr

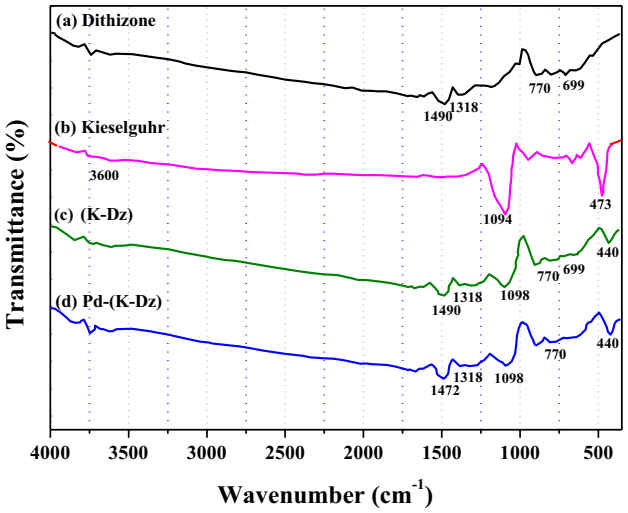


**Fig. 5** FTIR spectra of: **a** Dithizone, **b** Kieselguhr, **c** (K–Dz) composite, **d** Pd(II) loaded (K–Dz)

revealing that the immobilization of dithizone onto kieselguhr makes the structure of the surface slightly rougher.

On the other hand, the surface of (K–Dz) became smoother after the Pd(II) was loaded, as a result of the interaction of Pd(II) with the dithizone functional groups beside its sorption into the silica pores, Fig. 3f.

Figure 4a–c illustrates the EDX spectra of the blank kieselguhr, (K–Dz) and Pd-loaded immobilized kieselguhr, respectively. The detected nitrogen atom on the EDX spectrum of (K–Dz) indicates the successful immobilization of dithizone onto kieselguhr. The EDX spectrum after Pd(II) extraction supports that Pd(II) was adsorbed from an aqueous solution to the surface of the (K–Dz) composite.

The FTIR spectrum of free dithizone, typical kieselguhr, immobilized kieselguhr and Pd-loaded (K–Dz) composite are depicted in Fig. 5. Dithizone spectrum, Fig. 5a shows peaks at 1318 and 1490 $cm^{-1}$ that correspond in the same order to the stretching vibration of C–N and to the alkene bond (C=C) of the benzene ring [21]. The vibrational frequencies of the C–S and the aromatic C–H bond existed at 699 and 770 $cm^{-1}$, respectively [29]. For the kieselguhr spectrum, Fig. 5b two sharp bands were observed at 1094 and 473 $cm^{-1}$ are assigned to the stretching and bending vibrational mode of Si–O–Si, respectively [9]. Furthermore, a broad band appeared at 3600 $cm^{-1}$ ascribed to the stretching vibration of the –OH bond of the Si–OH group. However, in the case of immobilized kieselguhr Fig. 5c, the new bands at 1490, 1318, 699, 770 $cm^{-1}$ are attributed to the characteristic stretching vibrational band of dithizone. Moreover, the broadness of the peak at 1094 $cm^{-1}$ slightly shifted to 1098 $cm^{-1}$ affirming the successful immobilization process. On the other hand, After Pd(II) was loaded with (K–Dz) Fig. 5d, the peak at 1490 $cm^{-1}$ was shifted to 1472 $cm^{-1}$ as well the C–S band at 699 $cm^{-1}$ was deformed which may be attributed to the binding of Pd(II) with the functional groups of dithizone. In the meantime, it was observed no change in the vibrations of the Si–O–Si group of the kieselguhr indicating that its functional groups did not contribute to the sorption process [24].

## 3.2 Thermal Analysis

Thermogravimetric analysis (TGA) and differential thermal analysis (DTA) up to 600 °C of kieselguhr, dithizone immobilized kieselguhr before and after loaded with Pd metal ions were separately interpreted; to explore their thermal stability at elevated temperature state and represented in Fig. 6a and b. The TGA data of kieselguhr, Fig. 6a, illustrates that it had high thermal stability up to 600 °C with an overall mass loss of ~ 0.55%. On the other hand, the thermogram curve of dithizone immobilized kieselguhr, Fig. 6a, is characterized by two degradation stages with an overall mass reduction of 16.88% within 120 °C to 600 °C. An average mass loss value of 0.55% was noticed at temperature 110 °C which is due to the loss of weakly bound $H_2O$ molecules. This indicates that at high

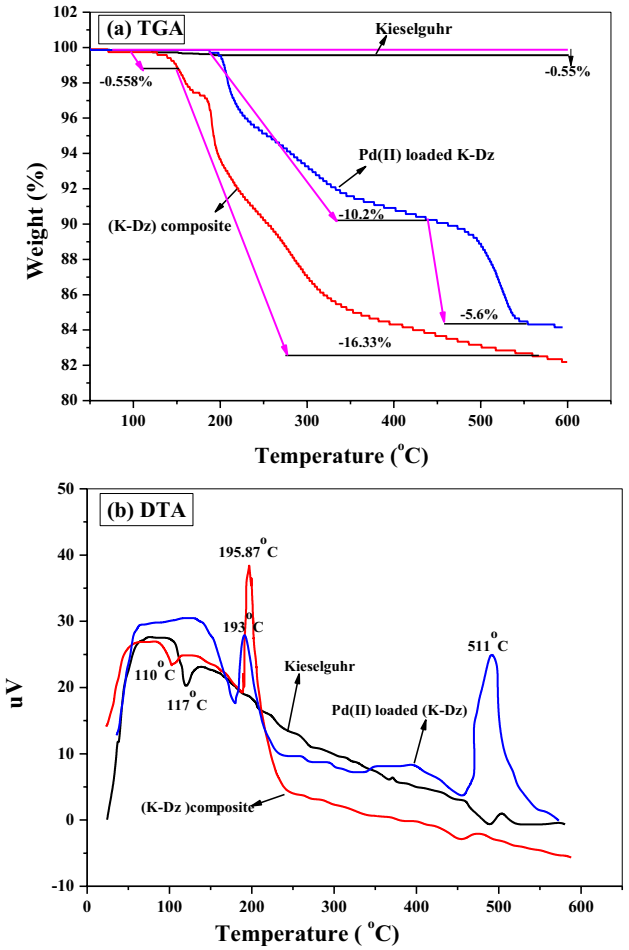


**Fig. 6** Thermal analysis: **a** TGA, **b** DTA curves of kieselguhr, (K–Dz) composite and Pd(II) loaded (K–Dz)

temperature, the prepared composite was almost stable. From the DTA curve of kieselguhr, Fig. 6b, only one endothermic peak at 117 °C was observed corresponding to the previous weight loss in the TGA curve which is attributed to the desorption of physically bound water molecules. In the DTA curve of (K-Dz) composite, Fig. 6b an endothermic peak was observed at 110 °C probably due to humidity, whereas the destruction of the immobilized dithizone caused an exothermic peak at 195.87 °C. From the literature data, the exothermic decomposition of dithizone has been reported in the range of 150–200 °C which is compatible with our data [30]. In the case of palladium loaded onto dithizone immobilized kieselguhr, Fig. 6b, a new exothermic peak was seen at temperature 511 °C corresponding to a mass loss of ~ 5.6% as calculated from the TGA curve, Fig. 6a. The overall mass loss of Pd(II) loaded (K–Dz) composite was 15.8% which is lower compared to the immobilized composite indicating that at high temperature, the prepared Pd(II) loaded (K–Dz) composite was almost stable. These observations are in good agreement with earlier

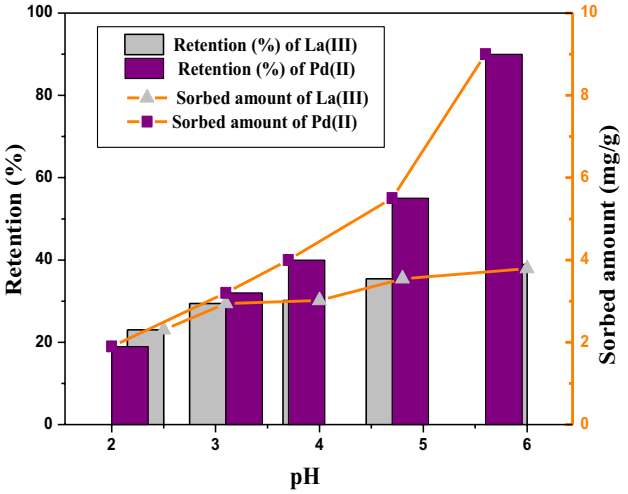


**Fig. 7** Effect of the solution pH on the sorption of Pd(II) and La(III) onto the (K–Dz) composite. ($C_o$ = 100 mg/L, Time = 15 min., V/m = 0.1 L/g, Temp. = 25 °C)

stated data [9]. These data support that, the presence of the metal ions resulted in thermal stability of the sorbent material.

## 4 Batch Sorption Examination

A batch sorption study was carried out to evaluate the efficacy of the immobilized kieselguhr with dithizone for extraction of Pd(II) and La(III) from an aqueous solution.

### 4.1 Effect of Hydrogen Ions Concentration

One of the most important factors influencing the sorption process is the concentration of hydrogen ions or pH. As it affects the speciation of the target metal ions as well as the charge sign of the active sites of the sorbent material. Therefore, the optimization of the solution pH is crucial [31]. The sorption of Pd(II) and La(III) onto (K–Dz) composite were investigated individually as a function of pH ranging from 2.0 to 6.0 and illustrated in Fig. 7. The percentage of Pd(II) and La(III) retained by the (K–Dz) composite increases as the solution pH is directed from acidic to alkaline with ultimate retention observed at pH 4.5–5.0 for Pd(II) and at pH 5.5 for La(III). This behavior may be explained due to the effect of pH solution on the species distribution of the metal ions with the solution pH and the protonation/deprotonation of the binding sites of the sorbent. The chemical behavior of Pd(II) in an aqueous solution was reported by Gianguzza et al. [32], they show that up to pH 5.5, Pd(II) chloride forms a stable complex $PdCl_x\left(H_2O\right)_{4-x}^{2-x}$, (x = 2, 3 or 4) while above pH 5.5, the sparingly soluble species $Pd(OH)Cl_3^{2-}$ starts to form. In the case of lanthanum [33], the predominant species is a trivalent cation, $La(H_2O)^{3+}$

at pH lower than 6.0. Whereas over this pH, it undergoes hydrolysis to form hydroxo complexes, $La(OH)^{2+}$; $La(OH)_2^+$, $La(OH)_3$ and $La(OH)_4^-$.

In an acidic medium, the competition between the hydronium ions and the concerned metals for the active sites of the sorbent material increased [34]. Hence, the interaction of the metals with the composite was suppressed due to the protonation of the –N and –S atoms of dithizone. Conversely, as the dithizone undergoes keto-enol tautomerism, when the concentration of hydronium ions is reduced, the active sites of the composite became deprotonated as well the thiol groups (–SH) of dithizone begin to dissociate ($pK_a = 4.5$) forming monobasic dithizonate ions ($HDz^-$) [20]. As a result, with increasing pH, the interaction of $Pd^{2+}$ and $La^{3+}$ cations with the $(HDz)^-$ immobilized on kieselguhr was increased. To overcome the Pd(II) and La(III) precipitation, the pH of the solution was not exceed 6.0. For this purpose, all subsequent experiments, the initial pH was maintained at 4.5.

Although La(III) has a higher electronic charge than Pd(II), the retention percent of La(III) by the immobilized kieselguhr is lower than Pd(II). The hard–soft acid–base (HSAB) theory can be used to explain this behavior. In contrast to Pd(II), lanthanide(III) ions are a hard acid that prefers to associate with donor atoms of ligand in the order: O >> N > S [35]. On the other hand, the dithizone ligand is classified as a soft and borderline base [21]. Hence, Pd(II) was selected over La(III) to interact with active sites of dithizone immobilized kieselguhr. The logarithm of the partition coefficient ($K_d$) for Pd(II) and La(III) onto the immobilized kieselguhr was plotted versus pH and is shown in Fig. 8. A linear relationship was obtained with slope values of 0.4 and 0.1 for Pd(II) and La (III), respectively. The slope values obtained were not related to the $M^{n+}/H^+$ exchange stoichiometric ratio indicating a complex interaction mechanism or electrostatic attraction rather than ion exchange, according to the following relationship [36]:

$$\text{Log } k_d = \text{ constant} + \text{ n pH} \quad (8)$$

where n refers to the number of proton released by adsorbing Pd(II) or La(III) by exchanging with the $H^+$ ions of the functional group of (K –Dz) composite.

Therefore, the reaction mechanism may be proposed in Scheme 1 as follows:

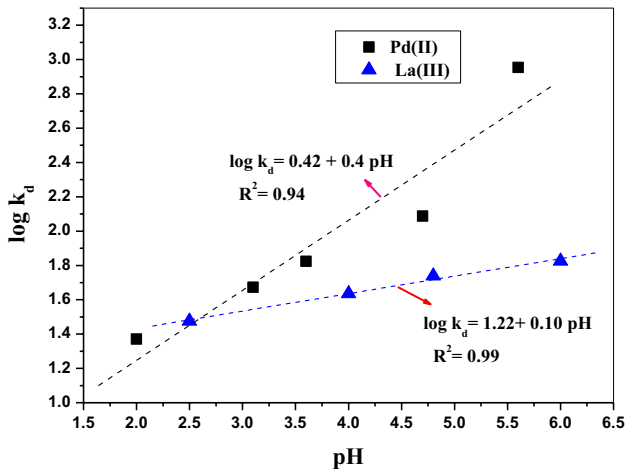


**Fig. 8** Plot of the logarithm of the partition coefficients against pH for sorption of Pd(II) and La(III) onto dithizone immobilized kieselguhr. ($C_o = 100$ mg/L, shaking time = 15 min., V/m = 0.1 L/g, Temp. = 25 °C)

## 4.2 Effect of the Composite Dose

The effect of the dithizone immobilized onto kieselguhr dosage on the sorbed amounts of Pd(II) and La(III) is presented in Fig. 9. As expected, the sorbed amount of Pd(II) and La(III) decreased as the dose of the composite increased from 0.02 to 0.125 g. As the sorbent mass increases, the available metal ions were not sufficient enough to react with the high density of the sorbent active sites resulting in a decrease in the sorption capacity [37]. Furthermore, it was observed that the sorption capacity of Pd(II) was 1.4 higher than La(III) at a sorbent mass

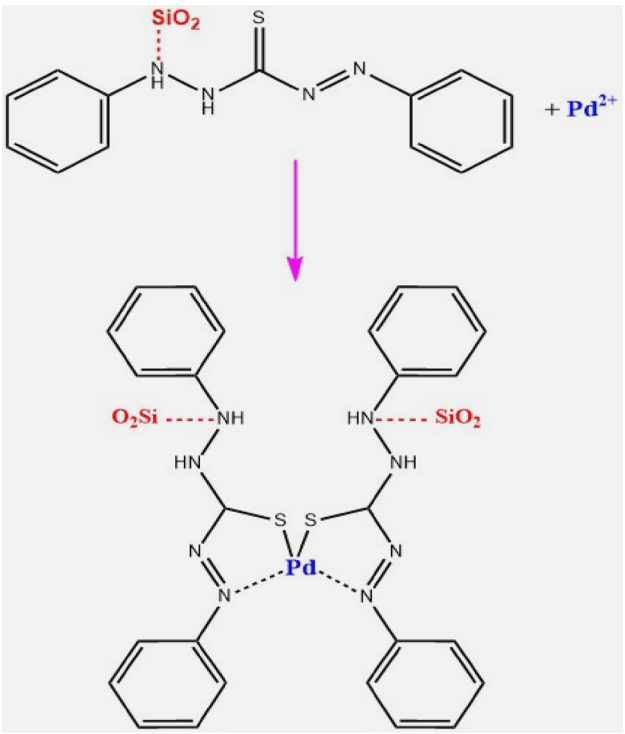


**Scheme 1** Schematic clarification of the formation process of Pd-loaded (K–Dz) composite

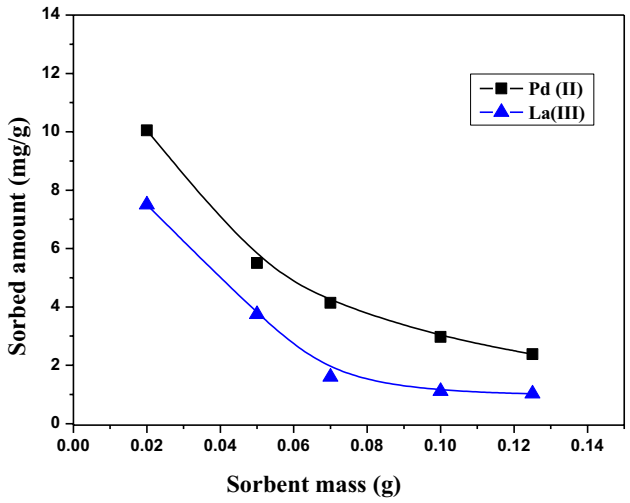


**Fig. 9** Effect of dithizone immobilized kieselguhr dose on the sorption of Pd(II) and La(III). ($C_o$ = 100 mg/L, pH 4.5, shaking time = 15 min., Temp. = 25 °C)

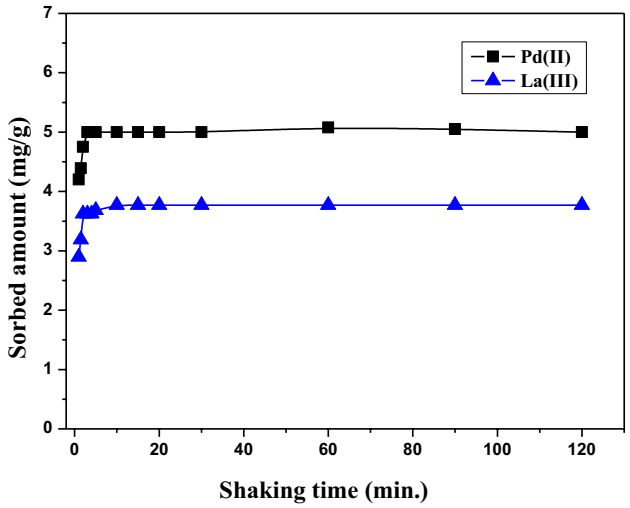


**Fig. 10** Effect of shaking time on the sorption of Pd(II) and La(III) onto dithizone immobilized kieselguhr. ($C_o$ = 100 mg/L, pH 4.5, V/m = 0.1 L/g, Temp. = 25 °C)

value of 0.05 g. This ratio was increased to 2.3 by increasing the sorbent dosage. As the sorbent accumulated in the solution, the steric bulkiness of the dithizone ligand may prevent its interaction with the bulky hydrated $La^{3+}$ ions [38]. Moreover, the active sites of the impregnated sorbent may be masked as a result of sorbent sintering when it is in a high concentration. Therefore, bulky hydrated La(III) could not access these hidden active sites unlike Pd(II) [39].

### 4.3 Retention Kinetics Study

The influence of shaking time on the amount of $Pd^{2+}$ and $La^{3+}$ ions sorbed onto dithizone immobilized kieselguhr was examined at different time intervals within two hours and is illustrated in Fig. 10. The time plot shows that the sorption rate was rapid where the reaction equilibrium was achieved after 10 min. while no change was observed in the sorption capacity of each metal ion with increasing the contact time. A similar result was reported by Marwani et al. [40]. The results demonstrate that at the beginning of the reaction, the active sites are more available to retain the metal ions compared to their amounts at a higher contact time.

The investigated data were analyzed by reaction and diffusion kinetic models to assess the rate-controlling step and the mechanism contributing to the sorption process. In this context, three non-linear kinetic models, namely pseudo-first-order (PFO), pseudo-second-order (PSO), and double–exponential (D–E) models were used to fit the experimental data [41, 42]. The choice of the most fitted model to the experimental data is based on the highest correlation coefficient and the lowest AIC values. Figure 11 displays the non-linear fitting of the kinetic data of the sorption of Pd(II) and La(III) using the aforementioned models and the obtained parameters accompanied by the $R^2$ and AIC values were presented in Table 1. The results elucidate that the retention kinetics of Pd (II) onto dithizone immobilized kieselguhr is well described by the PSO model since the acquired theoretical $q_e$ was close to its experimental value. Besides, the PSO fitting gave higher $R^2$ and lower AIC values compared to the PFO model. On the contrary, a better correlation was observed between the kinetic data of La(III) and the PFO model than the PSO model as the calculated $q_e$ from PFO was more consistent with the experimental data. Additionally, regarding the $R^2$ and AIC values, the PFO model can adequately represents the kinetic data of La(III). This behavior may be explained based on the surface activity of the donor atoms responsible for sorption and selective metal ions interaction [43]. The interaction of the dithizone with the kieselguhr occurs via electrostatic attraction between –NH group of the dithizone and Si–O–Si of the kieselguhr, leading to minimize the activity of the nitrogen donor atom for binding with La(III). Therefore, the retention of La(III) onto dithizone immobilized kieselguhr was most likely through electrostatic and physical interaction while the sorption of Pd(II) occurs via a complexation reaction. On the other hand, the D–E model also proposes the two-site mechanism as the sorbent contains two types of sorption sites accounting for dithizone and kieselgurhr. Therefore, the model parameters $D_1$, $K_{D_1}$ and $D_2$, $K_{D_2}$ represent the kinetic binding of the metals with kieselguhr and dithizone functional groups, respectively where the sorption of metal ions

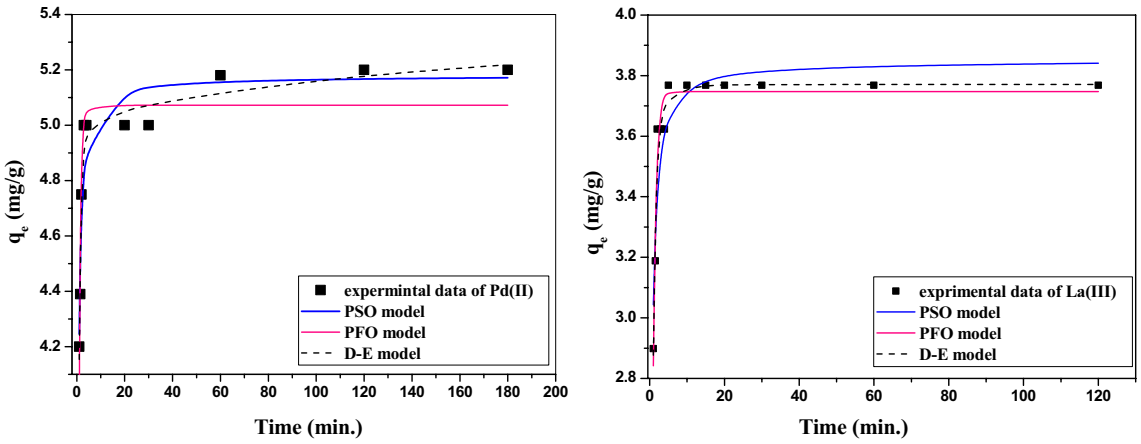


**Fig. 11** Non-linear PFO, PSO and D–E kinetic models for the sorption of Pd(II) and La(III) onto dithizone immobilized kieselguhr

**Table 1** Calculated parameters of the non-linear pseudo-first-order, pseudo-second-order and double exponential kinetic models for Pd(II) and La(III) ions sorbed onto dithizone immobilized kieselguhr composite

| Non-linear kinetic models equation | Model parameters | Pd(II) | La(III) |
|---|---|---|---|
| Pseudo-first-order | $q_{e,calc.}$ (mg/g) | 5.0 | 3.7 |
| $q_t = q_e\left(1 - e^{-k_1 t}\right)$ | $k_1$ ($min^{-1}$) | 1.56 | 1.42 |
| | $R^2$ | 0.87 | 0.95 |
| | AIC | − 38.0 | − 47.0 |
| | $q_{e,\ calc.}$ (mg/g) | 5.17 | 3.8 |
| Pseudo-second-order | $k_2$ (g $mg^{-1}$ $min^{-1}$) | 4.56 | 3.7 |
| $q_t = \frac{k_2 q_e^2}{(1+k_2 q_e t)}$ | $R^2$ | 0.91 | 0.87 |
| | AIC | − 41.0 | − 37.0 |
| | $q_{e,calac.}$ (mg/g) | 5.27 | 3.77 |
| Double exponential (D–E) | $D_1$ (mg/L) | 0.013 | 0.009 |
| $q_t = q_e - \frac{D_1}{m_{ads}} \exp(-k_{D_1} t - \frac{D_2}{m_{ads}} \exp\left(-k_{D_2} t\right)$ | $k_{D_1}$ ($min^{-1}$) | 0.008 | 0.263 |
| | $D_2$ (mg/L) | 0.123 | 0.168 |
| | $k_{D_2}$ ($min^{-1}$) | 1.05 | 1.50 |
| | $R^2$ | 0.965 | 0.96 |
| | AIC | − 45.0 | − 44.0 |
| $q_{e,\ experimental}$ (mg/g) | | 5.2 | 3.7 |

*Metal ion concentration = 100 mg/L

occurs rapidly on the first site while the metal ions are slowly adsorbed on the second site.

For further clarification in the regard to the retention mechanism of Pd(II) and La(III) onto the dithizone immobilized kieselguhr, the D–E model was applied as shown in Fig. 11 and the model parameters were illustrated in Table 1. It can be observed that the D–E model gave the best fit to the experimental data of Pd(II) and La(III) with $R^2 \geq 0.96$ and the lowest AIC values. Generally, the metal ions sorption takes place in two steps: a rapid step involves internal and external diffusion. Afterward, a slow step controls the sorption mechanism which may be due to the intraparticle diffusion. The $D_1$ value of Pd(II) is higher than that of La(III) which may be due to the difference in the reaction mechanism as the complexation of Pd(II) with the dithizone needs more time to complete the reaction. The rapid step depends mainly on the affinity of the metal ions for the sorbent and the exchange rate of the metal-ligand, while the slow step may be controlled by the intraparticle diffusion. The variation in the values of $K_{D_1}$ and $K_{D_2}$ for Pd(II) and La(III) suggests more than

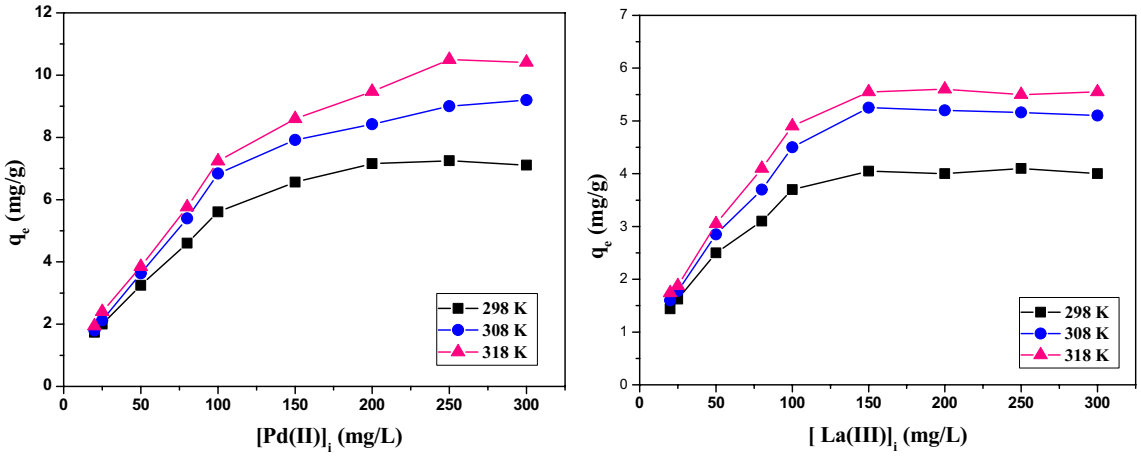


**Fig. 12** Effect of the initial concentration on the retained amounts of Pd(II) and La(III) onto (K–Dz) composite at different temperatures. (Shaking time = 15 min., pH 4.5, V/m = 0.1 L/g)

one diffusion mechanism involved in the sorption process [42].

### 4.4 Impact of the Initial Metals Concentrations

As it is known, the sorption capacity is strongly affected by the concentration of the adsorbate. Therefore, the sorption experiments of the initial concentrations of the single solution of Pd(II) and La(III) were implemented with different concentrations ranging from 20 to 300 mg/L at different temperatures under the optimum pH and time. Figure 12 illustrates that the amounts of Pd(II) and La(III) retained were enhanced by increasing their initial concentrations due to the satisfying amounts of the active sites on the (K–Dz) composite [21]. However, these sorption sites were minimized by increasing the amounts of the metal ions in the solution causing equilibrium and no further change was noticed in the retained amounts of Pd(II) and La(III) by increasing their concentrations to more than 200 mg/L. The maximum sorption capacity of the (K–Dz) composite shows a higher affinity for Pd(II) than for La(III), this may be related to the soft character of the dithizone ligand as well as, the square-planar geometry of Pd(II) leads to arrange in the frame of the composite sorbent other than La(III) which is characterized by tricapped trigonal prism [44]. Further, it was noticed that the temperature improves the sorption capacity of (K–Dz) composite for La(III) and Pd(II) indicating the sorption process was endothermic in nature.

## 5 Sorption Isotherms

The isotherm data can be appropriately analyzed by the Langmuir, Freundlich, Temkin, and Sips models to better understand the ideal mechanism of the sorption process. However, the Langmuir isotherm considers the adsorption as a chemical phenomenon, Freundlich, valid for physical adsorption and applies to adsorption on heterogeneous surfaces with the interaction between the adsorbed molecules. The Temkin model assumed that the binding energies distribute uniformly and the heat of energy decreases linearly with the surface coverage and is valid in the domain of an intermediate concentration range. On the other hand, Sips hybrid isotherm is a combination of the Langmuir and Freundlich isotherms and is valid for localized adsorption without adsorbate–adsorbate interactions. Sips model combines monolayer and multilayer adsorption as it minimizes to Freundlich at low concentration of the adsorbate while at high concentration the model predicts monolayer coverage.

The non-linear models form was expressed by the following equations [45]:

Non-linear Langmuir isotherm model:

$$q_e = \frac{Q_o b C_e}{\left(1 + bC_e\right)} \tag{9}$$

Non-linear Freundlich isotherm model:

$$q_e = K_f C_e^{1/n} \tag{10}$$

Non-linear Temkin isotherm model:

$$q_e = B_T \ln\left(A_T C_e\right) \tag{11}$$

Non-linear Sips isotherm model:

$$q_e = \frac{q_{m_s} k_s c_e^{m_s}}{1 + k_s C_e^{m_s}} \tag{12}$$

where $Q_o$ (mg/g) and b (L/mg) are the monolayer sorption capacity and Langmuir constant related to the binding

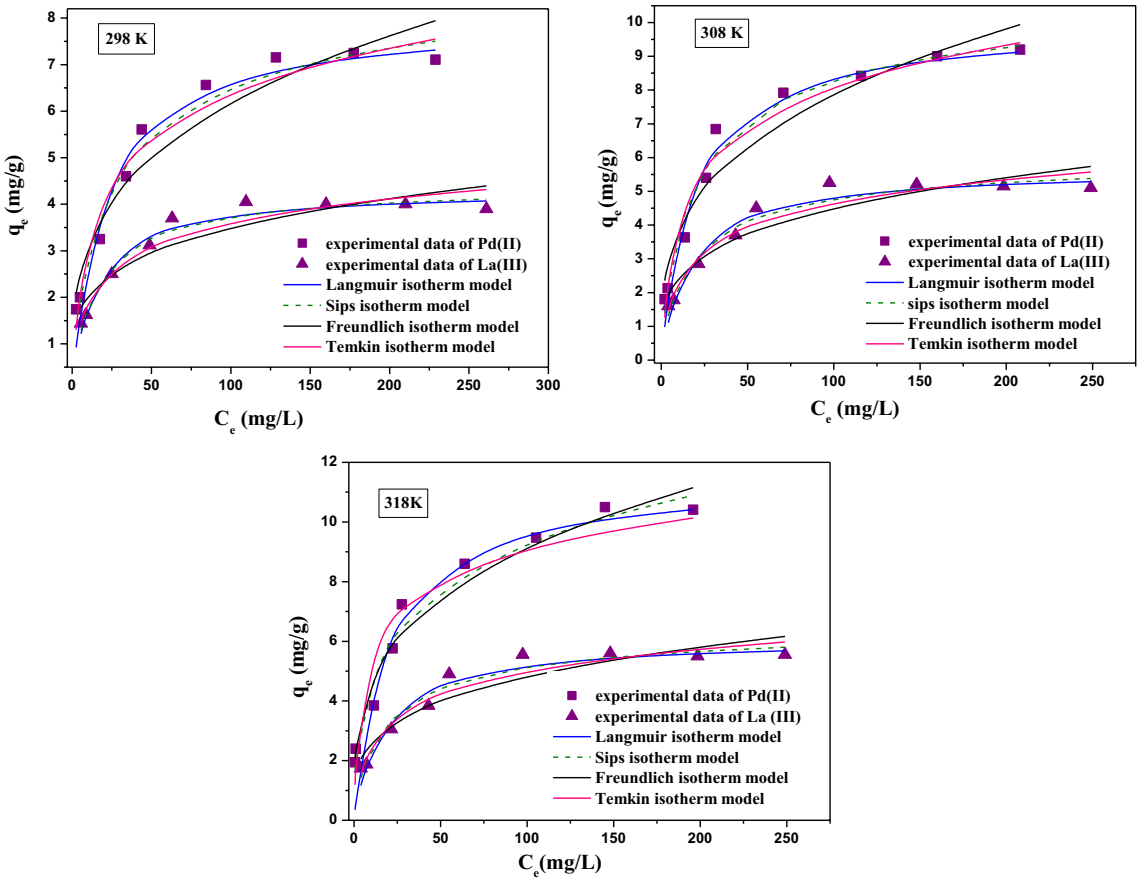


**Fig. 13** Non-linear regression analysis of the equilibrium sorption data of Pd(II) and La(III) onto (K–Dz) composite using Langmuir, Freundlich, Temkin and Sips isotherm models at 298 K, 308 K, and 318 K

energy. $K_f$ (mg/g $L^{1/n}$ $mg^{-1/n}$) and n means the Freundlich parameters associated with the sorption capacity and the bond energy of the sorbent–adsorbate, respectively. $B_T$ (kJ/mol) = RT/$b_T$ is constant where $b_T$ related to the heat of the sorption and $A_T$ (L/g) is the Temkin isotherm equilibrium binding constant. $q_{m_s}$ is the Sips maximum sorbent capacity (mg/g) while $k_s$ (L/mg) and $m_s$ express the Sips binding constant and the exponent of the model, respectively. The application of the aforementioned isotherm models for Pd(II) and La(III) at different temperatures were represented graphically in Fig. 13, whereas the output parameters with the regression values and the statistical criteria of the fitting were summarized in Table 2. As seen from the figure, the exponential trend of the Freundlich empirical equation showed a deviation from the experimental points of La(III) and Pd(II) at $C_i > 80$ mg/L. This was supported by lower regression values ($R^2$ varying from 0.87 to 0.93) as well as by higher values of AIC at all studied temperatures compared to the other tested models. However, the exponent, 1/n is less than one indicating that the sorption is suitable at low metal concentration and the sorption becomes more favorable as the concentration of the solid phase increases [46]. This may be attributed to the attractive force between the metal ions and the surface sites rapidly increasing compared to the repulsive force, arising from short and long-range Coulombic dipole repulsion, leading to a stronger tendency to bind with the surface sites [47]. As observed in Table 2, the numerical values of the Freundlich parameter relating to the sorption capacity, $K_f$ increases with the temperature and have values less than the Langmuir mono layer sorption capacity, $Q_o$. This indicates that $K_f$ may be considered as a comparative measure of a sorption capacity under particular conditions.

Regarding the Temkin isotherm model, the correlation coefficient had lower values in comparison with Langmuir and Sips model, Table 2. As noticed from the table, The sorption energies, $B_T$ values were positive and fall in the range of < 8.0 kJ/mole indicating that the sorption of Pd(II) and La(III) onto (K–Dz) composite involved both physical and chemisorption process [48].

Concerning to Langmuir and Sips model, they show more correspondence with the experimental data of Pd(II) and La(III) which gave the highest $R^2$ and lowest AIC values compared to Freundlich and Temkin models. According

**Table 2** Fitting of the non-linear isotherm models of Pd(II) and La(III) sorbed onto (K–Dz) composite at different temperatures with correlation factors ($R^2$) and Akaike criterion values (AIC)

| Model parameters | Pd(II) | | | La(III) | | |
|---|---|---|---|---|---|---|
| | 298 K | 308 K | 318 K | 298 K | 308 K | 318 K |
| *Langmuir* | | | | | | |
| $Q_o$ (mg/g) | 7.60 | 9.90 | 11.2 | 4.20 | 5.60 | 5.96 |
| b (L/mg) | 0.050 | 0.054 | 0.058 | 0.070 | 0.069 | 0.071 |
| $R^2$ | 0.966 | 0.975 | 0.94 | 0.97 | 0.96 | 0.93 |
| AIC | − 12.8 | − 10.6 | − 7.59 | − 27.1 | − 18.0 | − 12.5 |
| *Freundlich* | | | | | | |
| $K_f$ (mg/g $L^{1/n}$ $mg^{-1/n}$) | 1.56 | 1.89 | 2.40 | 1.18 | 1.50 | 1.40 |
| 1/n | 0.29 | 0.31 | 0.30 | 0.23 | 0.25 | 0.26 |
| $R^2$ | 0.93 | 0.93 | 0.96 | 0.87 | 0.90 | 0.91 |
| AIC | − 7.30 | − 2.8 | − 6.0 | − 15.5 | − 10.0 | − 9.5 |
| *Temkin* | | | | | | |
| $A_T$ (L/g) | 0.97 | 1.20 | 3.50 | 1.30 | 1.70 | 1.50 |
| $B_T$ (kJ/mol) | 1.77 | 1.48 | 1.79 | 3.35 | 2.6 | 2.78 |
| $R^2$ | 0.95 | 0.93 | 0.92 | 0.93 | 0.94 | 0.93 |
| AIC | − 12.18 | − 8.6 | − 1.0 | − 20.0 | − 15.5 | − 13.0 |
| *Sips* | | | | | | |
| $q_{ms}$ (mg/g) | 9.0 | 10.9 | 20.3 | 4.40 | 6.0 | 6.9 |
| $K_s$ (L/mg) | 0.086 | 0.083 | 0.096 | 0.087 | 0.089 | 0.12 |
| $m_s$ | 0.73 | 0.77 | 0.42 | 0.89 | 0.881 | 0.7 |
| $R^2$ | 0.978 | 0.98 | 0.97 | 0.97 | 0.97 | 0.95 |
| AIC | − 14.7 | − 11.0 | − 5.5 | − 26 | − 18.0 | − 13.7 |
| $q_{e,exp}$ (mg/g) | 7.3 | 9.25 | 10.55 | 4.05 | 5.3 | 5.56 |

to the Langmuir assumption, the metal ions are sorbed as a monolayer on a fixed number of surface sites that are identical with no interaction between the adsorbate. It was observed that the single layer of sorption capacity, $Q_o$ of Pd(II) and La(III) increased with the temperature which denotes that the functional groups associate in the sorption process instead of a set of similar surface sites [47]. The enhancement of $Q_o$ with the temperature may be expected as the saturation limit is influenced by many factors like the number of surface sites, the accessibility, the chemical state of the sites, and the strength of the binding between the metal ions and the surface sites of the sorbent. On the other hand, the Sips exponent, $m_s$ have values of $0 < m_s < 1$ suggesting that the Pd(II) and La(III) sorbed on (K–Dz) composite which has relatively homogenous binding sites [49]. Hence, the obtained maximum sorption capacities of Sips were slightly higher than those obtained from the Langmuir model which denotes that the (K–Dz) composite is not a perfectly flat surface. Therefore, the models that give the best description for the equilibrium data of La(III) and Pd(II) can be arranged in the order of the highest $R^2$ and the minimum AIC values in the following sequence:

Sips model > Langmuir model > Temkin model > Freundlich model.

## 6 Thermodynamic Studies

The temperature effect on the sorption behavior of Pd(II) and La(III) onto dithizone immobilized kieselguhr was examined by implementing the experiments at 298 K, 308 K, 318 K and 328 K. The thermodynamic parameters such as the enthalpy (ΔH°), the entropy (ΔS°) and the free Gibbs energy (ΔG°) were calculated from the subsequent relationships:

$$\ln k_d^\circ = \frac{\Delta S^\circ}{R} - \frac{\Delta H^\circ}{RT} \tag{13}$$

$$\Delta G^\circ = \Delta H^\circ - T\Delta S^\circ \tag{14}$$

where the dimensionless $k_d^\circ$ is calculated by multiplying the partition coefficient, $k_d$ (L/g) by the molecular weight of the adsorbate (g/mol) and the standard concentration of the adsorbate (1.0 mol/L) [31]. R is the universal gas constant (8.31 J/K.mol). The values of ΔH° and ΔS° were estimated from the slope and intercept of the plot of ln $k_d^\circ$ versus 1/T, respectively, and listed in Table 3. As observed from the table, The values of the ΔH° were positive indicating that the sorption process of Pd(II) and La(III) was endothermic

**Table 3** Thermodynamic parameters for Pd(II) and La(III) ions sorbed onto dithizone immobilized kieselguhr (K–Dz)

| Temperature (K) | Pd(II) | | | | | La(III) | | | | |
|---|---|---|---|---|---|---|---|---|---|---|
| | Ln $k_d^\circ$ | ΔG° (kJ/mol) | ΔH° (kJ/mol) | ΔS° (J/mol) | $R^2$ | Ln $k_d^\circ$ | ΔG° (kJ/mol) | ΔH° (kJ/mol) | ΔS° (J/mol) | $R^2$ |
| 298 | 10.03 | − 24.95 | 26.5 | 172.8 | 0.98 | 9.98 | − 24.80 | 16.30 | 138.19 | 0.97 |
| 308 | 10.56 | − 26.67 | | | | 10.32 | − 26.20 | | | |
| 318 | 10.74 | − 28.40 | | | | 10.48 | − 27.60 | | | |
| 328 | 11.05 | − 30.13 | | | | 10.60 | − 28.90 | | | |

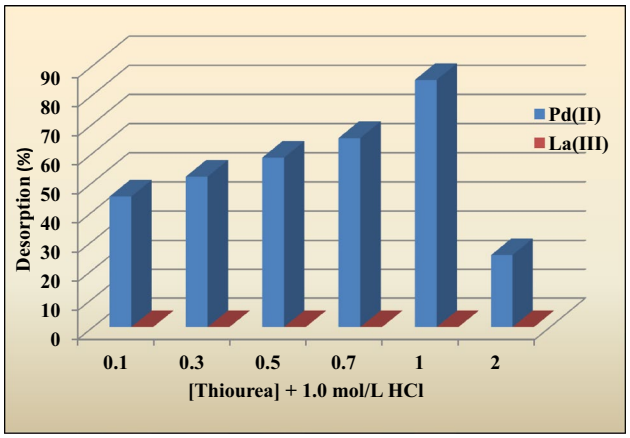


**Fig. 14** Desorption degree of Pd(II) and La(III) ions from (K–Dz) composite using different concentration of acidified thiourea as a desorbing agent

and the sorption was preferable at high temperatures [50]. The negative sign of ΔG° suggests the spontaneity of the sorption process. Besides, the increase in the randomness at the sorbent–adsorbate interface was approved by the positive values of ΔS°.

## 7 Desorption Studies

The desorption behavior of the metal ions makes it possible to reuse the sorbent and recycle the metals for further experiments continuously. The desorption of Pd(II) and La(III) from the loaded dithizone immobilized kieselguhr was performed using thiourea as adsorbing agent at concentrations ranging from (0.1 to 1.0 mol/L). The resultant data show that the Pd(II) was slightly back-extracted by 1.0 mol/L thiourea with a desorption percent of 15.0%, while thiourea had no impact on the desorption of La(III) from the stipulated composite. This behavior could be explained based on HSAB theory, where thiourea is considered as a soft base that is effectively coordinated with the palladium through the sulfur atom. However, the recovery of the loaded metals depends on using an eluting agent to form a more stable complex than their complex with the adsorbent [51]. It's noteworthy that, the effective sorbent requires a higher adsorption capacity and good desorption property. The synergistic effect of thiourea mixed with HCl on palladium (II) recovery was employed. In this concern, synergistic solutions of thiourea from (0.1 to 2.0 mol/L) + 1.0 mol/L HCl were used. As shown in Fig. 14, the recovery of Pd(II) increased with increasing the concentration of thiourea and most of Pd(II) returns back to the solution giving a desorption percent of approximately 80.0% at 1.0 mol/L thiourea mixed with 1.0 mol/L HCl. While the percentage of Pd(II) desorbed reduced at 2.0 mol/L thiourea concentration. Otherwise, the desorption percent was nil for La(III) ions at the same experimental conditions. This attitude was explained as in the hydrochloric acid medium, thiourea coordinated with Pd(II) chlorocomplex forming the stable complex $PdCl_2.2(NH_2)$ CS. Where the sulfur atom of thiourea is easily protonated in acidic conditions resulting in an electrophilic interaction between the protonated thiourea and Pd(II) chlorocomplex $(PdCl_4)^{2-}$ [52].

## 8 Application Study

Application of the results obtained in this work on the selective recovery of Pd(II) from the synthetic leach liquors of automotive catalysts was carried out after leaching the catalyst as explained in the experimental part. As a result, a synthetic solution consisting of the aforementioned elements was treated with a chloride solution at pH 4.5. The Ce(IV) was precipitated and filtered off. Sorption experiments were initially done by mixing 5.0 g of the (K–Dz) composite with the leach liquors as reported in the experimental section. The raffinate was found to contain Al(III), Pt(II), Rh(III) and La(III) as cationic complexes. After leaching, the leach solution and the remaining insoluble solid residue were separated by filtration, and the solid residue was used for the elution step. Then, the desorption of Pd(II) ions from the adsorbed resin were then carried out successfully by using acidified thiourea (mixture from 1.0 mol/L HCl + 1.0 mol/L

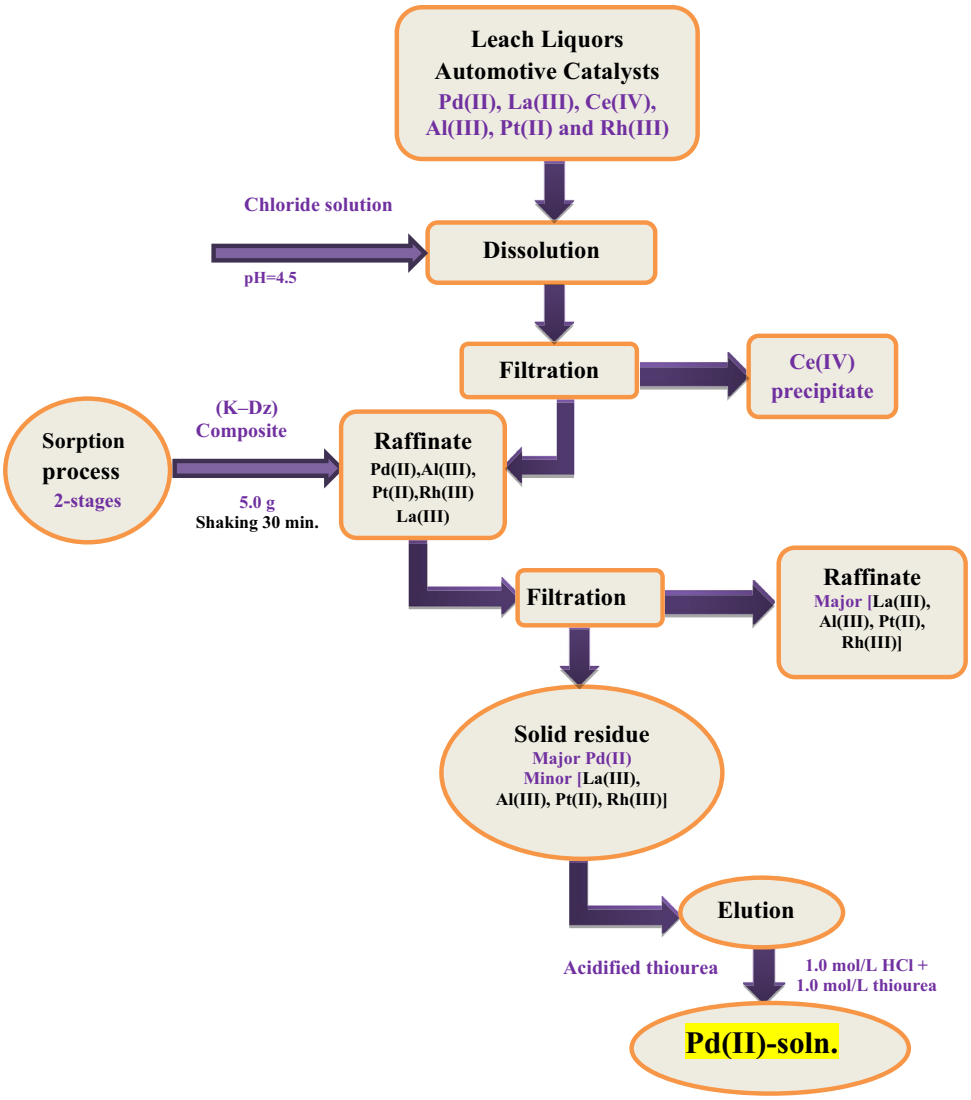


**Fig. 15** Flow chart for the sequential separation of Pd(II) from simulated leach liquor solution of automotive catalyst in chloride solution

**Table 4** Long-term sorption sustainability of (K–Dz) composite

| Storage time (months) | Sorption percent of Pd(II) (%) | Sorption efficiency loss (%) |
|---|---|---|
| Freshly prepared | 55.0 | 0.0 |
| 3.0 | 45.1 | 18.8 |
| 6.0 | 22.0 | 60.0 |

thiourea) solution leaving Al(III) and other elements poorly eluted. The schematic diagram explaining the proposed process for the efficient separation of Pd(II) from automotive catalyst leach liquor is shown in Fig. 15.

## 9 Long-Term Sorption Sustainability of (K–Dz) Composite

The long-term stability of the (K–Dz) composite was checked in terms of the sorption percent of Pd(II). A series of sorption tests were conducted under the same conditions with a new prepared composite, stored away from direct sunlight for 3.0 and 6.0 months. The results were listed in Table 4. It is clearly shown that the sorption percent of Pd(II) by the composite decreases as the storage time increases. At 6.0 months of storage, the sorption efficiency of the (K–Dz) composite dropped to about 40.0% of its initial value with a 60.0% sorption efficiency loss. This decay may be due to the hot weather and the diffusion of the original light on the dithizone sulfur group, which is sensitive to oxidation. These

results concerning the stability of the composite are better than that observed by Wu et al. [53] who reported that the prepared Amberlite XAD-2 functionalized with dithizone could be stable for about one month of storage. On the other hand, Yin et al. [54] stated that the dithizone functionalized with (Zobax XDB-C18) column has short-term stability for about only one week. In this concern, the long-term stability and sustainability of the studied composite are more favorable for further applications.

## 10 Conclusions

In this research, diphenylthiocarbazone or dithizone immobilized onto kieselguhr was successfully synthesized via physical impregnation process which was approved by XRD, SEM, EDX, (TGA/DTA) and FTIR analysis. As revealed by SEM analysis, dithizone impregnation did not modify the surface morphology of the kieselguhr. The sorption capability of (K–Dz) composite was tested to retain Pd(II) and La(III) from a single aqueous solution by a batch technique. The amounts of Pd(II) and La(III) possessed increased with increasing the solution pH, initial metal ions concentration, contact time, and temperature. (K–Dz) composite exhibited excellent efficiency for Pd(II) uptake in comparison with La(III), from an aqueous medium according to the hard–soft acid–base (HSAB) theory. Kinetic study shows that the sorption of Pd(II) onto (K–Dz) composite follows a pseudo-second-order conversely to La(III) which follows pseudo-first-order indicating that the sorption depends on the surface activity of the donor atoms responsible for sorption and selective metal ions interaction. The adsorption isotherm of Pd(II) and La(III) was well represented by the Sips and Langmuir isotherm model with higher values of their correlation coefficients and minimum values of Akakie criterion compared to Freundlich and Temkin isotherm models, suggesting that the sorption occurred onto relatively homogenous binding sites. The negative value of the change in Gibbs free energy, $\Delta G^{o}$, indicates that the adsorption process is spontaneous. While the positive value of enthalpy changes, $\Delta H^{o}$, supports the endothermic nature of the sorption process. The positive value of $\Delta S^{o}$ indicates the high degree of randomness of the system between sorbent surface and sorbate species in solution. The sorbent can be efficiently regenerated by synergistic solutions of acidified thiourea (at 1.0 mol/L thiourea mixed with 1.0 mol/L HCl) as an effective eluent forming the stable complex $PdCl_2.2(NH_2)CS$. Finally, the above results suggest that (K–Dz) composite can be used as a potential adsorbent for the efficient separation of Pd(II) and La(III) ions from a simulated automotive catalyst leachate solution, under the used experimental conditions.

**Acknowledgements** The authors are thankful and grateful to Prof. Hisham Foaud Aly for kindly supplying kieselguhr. This research is funded by the Egyptian Atomic Energy Authority and did not receive any specific grant from funding agencies in the public, commercial, or not-for profit sectors.

**Funding** Open access funding provided by The Science, Technology & Innovation Funding Authority (STDF) in cooperation with The Egyptian Knowledge Bank (EKB). The authors have not disclosed any funding.

## Declarations

**Conflict of interest** The authors have no relevant financial or non-financial interests to disclose.



## References

1. Q. Ricoux, V. Bocokic, J.P. Méricq, D. Bouyer, S.V. Zutphen, C. Faur, Selective recovery of palladium using an innovative functional polymer containing phosphine oxide. Chem. Eng. J. **264**(15), 772–779 (2015). https://doi.org/10.1016/j.cej.2014.11.139
2. K.K. Singh, R. Ruhela, A. Das, M. Kumar, A.K. Singh, R.C. Hubli, P.N. Bajaj, Separation and recovery of palladium from spent automobile catalyst dissolver solution using dithiodiglycolamide encapsulated polymeric beads. J. Environ. Chem. Eng. **3**(1), 95–103 (2015). https://doi.org/10.1016/j.jece.2014.11.002
3. S. Ning, S. Zhang, W. Zhang, J. Zhou, S. Wang, X. Wang, Y. Weia, Separation and recovery of Rh, Ru and Pd from nitrate solution with a silica based IsoBu-BTP/$SiO_2$-P adsorbent. Hydrometallurgy **191**, 105207 (2020). https://doi.org/10.1016/j.hydromet.2019.105207
4. H.T. Truong, M.S. Lee, Separation of Pd(II) and Pt(IV) from hydrochloric acid solutions by solvent extraction with Cyanex 301 and LIX 63. Miner. Eng. **115**, 13–20 (2018). https://doi.org/10.1016/j.mineng.2017.10.001
5. M. Soylak, N.D. Erdogan, Copper(II)-rubeanic acid coprecipitation system for separation-preconcentration of trace metal ions in environmental samples for their flame atomic absorption spectrometric determinations. J. Hazard. Mater. **137**(2), 1035–1041 (2006). https://doi.org/10.1016/j.jhazmat.2006.03.031
6. P.P. Sun, T.Y. Kim, B.J. Min, H.I. Song, S.Y. Cho, Recovery of platinum from chloride leaching solutions of spent reforming catalysts by ion exchange. Mater. Trans. **56**(5), 738–742 (2015). https://doi.org/10.2320/matertrans.M2015027
7. M. Wojnicki, Kinetic studies of the sorption process of Pd(II) chloride complex ions from diluted aqua solutions using commercially available activated carbon. React. Kinet. Mech. Catal. **122**(1), 177–192 (2017). https://doi.org/10.1007/s11144-017-1233-8
8. Y.H. Zhao, J.T. Geng, J.C. Cai, Y.F. Cai, Adsorption performance of basic fuchsin on alkali-activated diatomite. Adsorpt.

Sci. Technol. **38**(5–6), 151–167 (2020). https://doi.org/10.1177/0263617420922084
9. ShSh. Emam, M.S. Gasser, N.E. El-Hefny, W.H. Mahmoud, H.F. Aly, Sorption of certain lanthanides by kieselguhr loaded with Cyanex 572 from sulfate medium. J. Rare Earths (2019). https://doi.org/10.1016/j.jre.2019.06.002
10. M. Yamada, M.R. Gandhi, Y. Kondo, K. Haga, A. Shibayama, F. Hamada, Selective sorption of palladium by thiocarbamoyl-substituted thiacalix[n]arene derivatives immobilized on amberlite resin: application to leach liquors of automotive catalysts. RSC Adv. **5**(74), 60506–60517 (2015). https://doi.org/10.1039/c5ra07921g
11. R. Ruhela, K. Singh, B.S. Tomar, T.K. Shesagiri, M. Kumar, R.C. Hubli, A.K. Suri, Amberlite XAD-16 functionalized with 2-Acetyl Amide group for the solid phase extraction and recovery of palladium from high level waste. Ind. Eng. Chem. Res. **52**(15), 5400–5406 (2013). https://doi.org/10.1021/ie3021126
12. A.R.L. Spies, F. Wewers, Equilibrium, kinetics and thermodynamics studies of Cd sorption onto a dithizone-impregnated Amberchrom CG-300m polymer resin. Arab. J. Chem. **13**(4), 5050–5059 (2020). https://doi.org/10.1016/j.arabjc.2020.02.004
13. K. Omri, N. Alonizan, Effects of ZnO/Mn concentration on the micro-structure and optical properties of ZnO/Mn–$TiO_2$ nanocomposite for applications in photo catalysis. Inorg. Organomet. Polym. Mater. **29**, 203–212 (2019). https://doi.org/10.1007/s10904-018-0979-4
14. K. Omri, F. Alharb, Microstructural properties and improvement in photoluminescence thermometry of Mn-activated single-phased Zn–SO–Mn phosphors. J. Mater. Sci. **32**, 24229–24239 (2021). https://doi.org/10.1007/s10854-021-06888-1
15. K. Omri, I. Najeh, L. El Mir, Influence of annealing temperature on the microstructure and dielectric properties of ZnO nanoparticles. Ceram. Int. **42**, 8940–8948 (2016). https://doi.org/10.1016/j.ceramint.2016.02.151
16. K. Omri, S. Gouadria, Dielectric investigation and effect of low copper doping on optical and morphology properties of ZO-Cu nanoparticles. J. Mater. Sci. **32**, 17021–17031 (2021). https://doi.org/10.1007/s10854-021-06268-9
17. L. Xu, H. Wang, Z. Chu, L. Cai, H. Shi, C. Zhu, D. Pan, J. Pan, X. Fei, Y. Lei, Temperature-responsive multilayer films of micelle-based composites for controlled release of a third-generation EGFR inhibitor. ACS Appl. Polym. Mater. **2**(2), 741–750 (2020). https://doi.org/10.1021/acsapm.9b01051
18. L. Xu, X. Zhang, Z. Chu, H. Wang, Y. Li, X. Shen, L. Cai, H. Shi, C. Zhu, J. Pan, D. Pan, Temperature-tesponsive multilayer films based on block copolymer-coated silica nanoparticles for long-term release of Favipiravir. ACS Appl. Nano Mater. **4**(12), 14014–14025 (2021). https://doi.org/10.1021/acsanm.1c03334
19. L. Xu, Z. Chu, H. Wang, L. Cai, Z. Tu, H. Liu, C. Zhu, H. Shi, D. Pan, J. Pan, X. Fei, Electrostatically assembled multilayered films of biopolymer enhanced nanocapsules for on-demand drug release. ACS Appl. Bio Mater. **2**(8), 3429–3438 (2019). https://doi.org/10.1021/acsabm.9b00381
20. Z. Marzenko, *Spectrophotometric Determination of Elements* (Wiley, New York, 1986)
21. M. Mudasir, R.A. Baskara, A. Suratman, K.S. Yunita, R. Perdana, W. Puspitasari, Simultaneous adsorption of Zn(II) and Hg(II) Ions on selective adsorbent of dithizone-immobilized bentonite in the presence of Mg(II) ion. J. Environ. Chem. Eng. **8**(4), 104002 (2020). https://doi.org/10.1016/j.jece.2020.104002
22. A.K. Nayak, A. Pal, Development and validation of an adsorption kinetic model at solid-liquid interface using normalized Gudermannian function. J. Mol. Liq. **276**, 67–77 (2019). https://doi.org/10.1016/j.molliq.2018.11.089
23. T. Kimuro, M.R. Gandhi, U.M.R. Kunda, F. Hamada, M. Yamada, Palladium(II) sorption of a diethylphosphate-modified thiacalix[6]arene immobilized on amberlite resin. Hydrometallurgy **171**, 254–261 (2017). https://doi.org/10.1016/j.hydromet.2017.05.022
24. K. Li, J. Chen, D. Zou, Extraction and recovery of cerium from rare earth ore by solvent extraction. in *Cerium Oxide-Applications and Attributes* (2019)https://doi.org/10.5772/intechopen.79225
25. H.M. Yu, H. Song, M.L. Chen, Dithizone immobilized silica gel online preconcentration of trace copper with detection by flame atomic absorption spectrometry. Talanta **85**(1), 625–630 (2011). https://doi.org/10.1016/j.talanta.2011.04.039
26. Y. Wang, J. Xie, Y. Wu, H. Ge, X. Hu, Preparation of a functionalized magnetic metal–organic framework sorbent for the extraction of lead prior to electrothermal atomic absorption spectrometer analysis. J. Mater. Chem. A **1**(31), 8782 (2013). https://doi.org/10.1039/C3TA11178D
27. A.S. Saqezi, M. Kermanian, A. Ramazani, S. Sadighian, synthesis of grapheneoxide/iron oxide/Au nanocomposite for quercetin delivery. J. Inorg. Organomet. Polym. Mater. (2022). https://doi.org/10.1007/s10904-022-02259-3
28. O.A. Abdel Moamen, H.S. Hassan, W.F. Zaher, Taguchi L16 optimization approach for simultaneous removal of $Cs^+$ and $Sr^{2+}$ ions by a novel scavenger. Ecotoxicol. Environ. Saf. **189**, 110013 (2020). https://doi.org/10.1016/j.ecoenv.2019.110013
29. A. Khan, S. Badshah, C. Airoldi, Environmentally benign modified biodegradable chitosan for cation removal. Polym. Bull. **72**(2), 353–370 (2014). https://doi.org/10.1007/s00289-014-1278-z
30. B.N. Huda, E.T. Whaynu, M. Mudasir, Eco-friendly immobilization of dithizone on coal bottom ash for the adsorption of lead(II) ion from water. Results Eng. **10**, 100221 (2021). https://doi.org/10.1016/j.rineng.2021.100221
31. X. Liu, H. Zhang, Y. Luo, R. Zhu, H. Wang, B. Huang, Sorption of oxytetracycline in particulate organic matter in soils and sediments: roles of pH, ionic strength and temperature. Sci. Total Environ. **714**, 136628 (2020). https://doi.org/10.1016/j.scitotenv.2020.136628
32. A. Gianguzza, D. Milea, A. Pettignano, S. Sammartano, Palladium(II) sequestration by phytate in aqueous solution. Speciation analysis and ionic medium effects. Environ. Chem. **7**(3), 259–267 (2010). https://doi.org/10.1071/EN10008
33. S. Iftekhar, D.L. Ramasamy, V. Srivastava, M.B. Asif, M. Sillanpaa, Understanding the factors affecting the adsorption of Lanthanum using different adsorbents: a critical review. Chemosphere **204**, 413–430 (2018). https://doi.org/10.1016/j.chemosphere.2018.04.053
34. B. Hu, L. Wu, M. Ou, X. Wang, Y. Tang, Sorption studies of chromium(VI) onto cerium/ferroferric oxide composites. J Inorg. Organomet. Polym. **31**, 2627–2637 (2021). https://doi.org/10.1007/s10904-021-01944-z
35. M. Zabiszak, M. Nowak, Z. Hnatejko, J. Grajewski, K. Ogawa, M.T. Kaczmarek, R. Jastrzab, Thermodynamic and spectroscopic studies of the complexes formed in tartaric acid and lanthanide(III) ions binary systems. Molecules **25**(5), 1121 (2020). https://doi.org/10.3390/molecules25051121
36. K.Z. Elwakeel, M.F. Hamza, E. Guibal, Effect of agitation mode (mechanical, ultrasound and microwave) on uranium sorption using amine- and dithizone-functionalized magnetic chitosan hybrid materials. Chem. Eng. J. **411**, 128553 (2021). https://doi.org/10.1016/j.cej.2021.128553
37. N. Das, D. Das, Recovery of rare earth metals through biosorption: an overview. J. Rare Earths **31**(10), 933–943 (2013). https://doi.org/10.1016/S1002-0721(13)60009-5
38. M. Takagi, T. Omori, S. Matsuo, S. Matsuno, K. Ueno, S. Ide, Sulfonamides. A new class of chelating agents of potential utility in analytical and separation chemistry. Chem. Lett. **9**(4), 387–390 (1980). https://doi.org/10.1246/cl.1980.387
39. G. Raharjo, I. Tahir, E.T. Wahyuni, Immobilization of dithizone onto chitin isolated from Prawn seawater shells (*P. merguensis*)

and its preliminary study for the adsorption of Cd(II) Ion. J. Phys. Sci. **19**(1), 63–78 (2008)
40. H.M. Marwani, H.M. Albishri, T.A. Jalal, E.M. Soliman, Activated carbon immobilized dithizone phase for selective adsorption and determination of gold(III). Desalin. Water Treat. **45**(1–3), 28–135 (2012). https://doi.org/10.1080/19443994.2012.692019
41. T. Yousefi, M.A. Mohsen, H.R. Mahmudian, M. Torab-Mostaedi, M.A. Moosavian, H. Aghayan, Removal of Pb(II) by Modified natural adsorbent; thermodynamics and kinetics studies. J. Water Environ. Nanotechnol. **3**(3), 265–272 (2018). https://doi.org/10.22090/jwent.2018.03.007
42. L.A. Attia, M.A. Youssef, O.A. Abdel Moamen, Feasibility of radioactive cesium and europium sorption using valorized punica granatum peel: kinetic and equilibrium aspects. Sep. Sci. Technol. **56**(2), 217–232 (2021). https://doi.org/10.1080/01496395.2019.1708111
43. M.E. Mahmoud, M.M. Osman, M.E. Amer, Selective pre- concentration and solid phase extraction of mercury(II) from natural water by silica gel-loaded dithizone phases. Anal. Chim. Acta **415**(1–2), 33–40 (2000). https://doi.org/10.1016/S0003-2670(00)00839-4
44. S. Wang, T. Vincent, J.C. Roux, C. Faur, E. Guibal, Pd(II) and Pt(IV) sorption using alginate and algal-based beads. Chem. Eng. J. **313**, 567–579 (2017). https://doi.org/10.1016/j.cej.2016.12.039
45. H.S. Ta, K.L. Van, T.T.L. Thi, D.H. Nguyen, Thermodynamic studies on the adsorption of phenol from aqueous solution by coffee husk activated carbon. Egypt. J. Chem. **64**(5), 2355–2367 (2021). https://doi.org/10.21608/ejchem.2021.30318.2648
46. A.B. Kanagare, K.K. Singh, K.K. Bairwa, R. Ruhela, V.S. Shinde, M. Kumar, A.K. Singh, Dithiodiglycolamide impregnated XAD-16 beads for separation and recovery of palladium from acidic waste. J. Environ. Chem. Eng. **4**(3), 3357–3363 (2016). https://doi.org/10.1016/j.jece.2016.06.031
47. R.O. Abdel Rahman, H.A. Ibrahim, M. Hanafy, N.M. Abdel Monem, Assessment of synthetic zeolite Na A-X as sorbing barrier for strontium in a radioactive disposal facility. Chem. Eng. J. **157**(1), 100–112 (2010). https://doi.org/10.1016/j.cej.2009.10.057
48. A. Murcia-Salvador, J.A. Pellicer, M.I. Fortea, V.M. Gómez-López, M.I. Rodríguez-López, E. Núñez-Delicado, J.A. Gabaldón, Adsorption of direct blue 78 using chitosan and cyclodextrins as adsorbents. Polymers **11**(6), 1003 (2019). https://doi.org/10.3390/polym11061003
49. R. Saadi, Z. Saadi, R. Fazaeli, N.E. Fard, Monolayer and multilayer adsorption isotherm models for sorption from aqueous media. Korean J. Chem. Eng. **32**(5), 787–799 (2015). https://doi.org/10.1007/s11814-015-0053-7
50. A. Abbasi, R. Davarkhah, A. Avanes, A. Yadollahi, M.G. Maragheh, H. Sepehrian, Development of nanoporous alumino-borosilicate as a novel matrix for the sorption and stable immobilization of cesium ions. J Inorg. Organomet. Polym. **30**, 369–378 (2020). https://doi.org/10.1007/s10904-019-01195-z
51. O.N. Kononova, A.M. Melnikov, D.S. Demitrichenko, Simultaneous ion exchange recovery and subsequent separation of platinum(II, IV), rhodium(III), and nickel(II) from chloride and sulfate-chloride solutions. Solvent Extr. Ion Exch. **31**, 306–319 (2013). https://doi.org/10.1080/07366299.2012.757133
52. V. Mohdee, V. Parasuk, U. Pancharoen, Synergistic effect of thiourea and HCl on palladium (II) recovery: an investigation on chemical structures and thermodynamic stability via DFT. Arab. J Chem. **14**, 103196 (2021). https://doi.org/10.1016/j.arabjc.2021.10319
53. D. Wu, A. Wang, L. Guo, Synthesis and application of Amberlite XAD-2 functionalized with dithizone for field preconcentration and separation of trace cadmium in seawater. Anal. Sci. **22**, 1245–1248 (2006). https://doi.org/10.2116/analsci.22.1245
54. Y.G. Yin, M. Chen, J.F. Peng, J.F. Liu, G.B. Jiang, Dithizone-functionalized solid phase extraction-displacement elution-high performance liquid chromatography inductively coupled plasma mass spectrometry for mercury speciation in water samples. Talanta **81**, 1788–1792 (2010). https://doi.org/10.1016/j.talanta.2010.03.039